Slip Morphology of Elastic Strips on Frictional Rigid Substrates

Tomohiko G. Sano,[1,2] Tetsuo Yamaguchi,[3,4] and Hirofumi Wada[1]
[1]Department of Physical Sciences, Ritsumeikan University, Kusatsu, Shiga 525-8577, Japan
[2]Research Organization of Science and Technology, Ritsumeikan University, Kusatsu, Shiga 525-8577, Japan
[3]Department of Mechanical Engineering, Kyushu University, Fukuoka 819-0395, Japan
[4]International Institute for Carbon-Neutral Energy Research, Kyushu University, Fukuoka 819-0395, Japan
(Received 4 July 2016; revised manuscript received 15 February 2017; published 26 April 2017)

The morphology of an elastic strip subject to vertical compressive stress on a frictional rigid substrate is investigated by a combination of theory and experiment. We find a rich variety of morphologies, which—when the bending elasticity dominates over the effect of gravity—are classified into three distinct types of states: pinned, partially slipped, and completely slipped, depending on the magnitude of the vertical strain and the coefficient of static friction. We develop a theory of elastica under mixed clamped-hinged boundary conditions combined with the Coulomb-Amontons friction law and find excellent quantitative agreement with simulations and controlled physical experiments. We also discuss the effect of gravity in order to bridge the difference in the qualitative behaviors of stiff strips and flexible strings or ropes. Our study thus complements recent work on elastic rope coiling and takes a significant step towards establishing a unified understanding of how a thin elastic object interacts vertically with a solid surface.

DOI: 10.1103/PhysRevLett.118.178001

Introduction.—Contact between slender objects gives rise to complex structures and behaviors in nature [1–15], including DNA ejection from bacteriophages [2], the folding of sheetlike tissues in developmental biology [3,4], and the coiling of plant tendrils or roots [5–7]. Examples in daily life [16–25] include hair brushing, arranging pony tails [16], applying gift-wrap ribbons [17], tying shoelaces [18], rucks in a rug [19,20], coiling elastic or liquid ropes [21–25], or the use of polymer brushes [26], biomimetics [27–31], and coiled tubing in industry [32]. Since frictional effects [33–37] play an important role when slender objects are in contact with each other [15], the interplay between friction and the elasticity of thin objects is currently a central topic in this field of research.

A fundamental process common to a variety of the problems listed above is the postbuckling behavior of an elastic strip [38–43] that is subject to a vertical compressive stress on a rigid substrate [Fig. 1(a)]. Initially, the strip takes the form of a planar elastica, but upon further compression, its free tip may slip [Fig. 1(b)]. The direction of this slippage is opposite to the direction of the initial buckling (which is determined by spontaneous symmetry breaking), as the slip acts to reduce the overall curvature of the strip. Despite the familiarity, simplicity, and fundamental importance of this prototypical phenomenon, its underlying physics remains unclear thus far. For example, several unanswered questions are when and how does the strip slip, what factors determine the slip length, and what are the possible resultant forms of the elastica? To answer these basic questions, it is necessary to disentangle the complex interplay between elasticity, geometry, friction, and gravity.

In this Letter, we investigate the above-outlined problem using numerical, analytical, and experimental approaches. The frictional interaction between the strip's tip and the surface of the substrate is modeled according to the Coulomb-Amontons law [33–37], which states that the tip of the strip remains stationary if the frictional force from the substrate, $\vec{\mathcal{F}} = (\mathcal{F}_x, \mathcal{F}_y)$, satisfies

$$|\mathcal{F}_x| \le \mu \mathcal{F}_y, \tag{1}$$

where μ represents the coefficient of static friction. Equation (1) suggests that the instantaneous shape of an elastica determines its own boundary condition. This feature is a particular characteristic of our system and differs from the behavior in a standard setup employed in previous

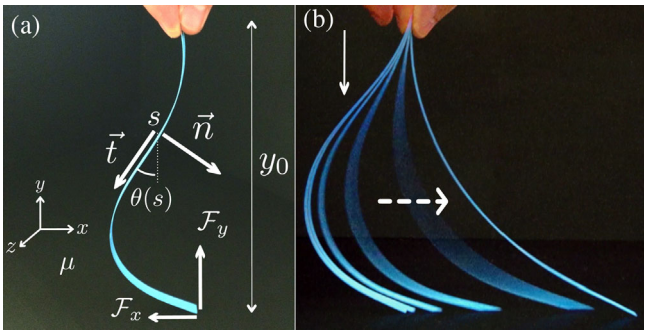

FIG. 1. Typical morphology of a strip on a solid surface. (a) Geometry of our system and definition of the key variables. $\vec{t}$ and $\vec{n}$ are the unit tangent and normal vectors of the strip center line, respectively. $\theta(s)$ represents the angle of $\vec{t}$ measured from the y axis. (Note that θ here is defined negative.) The strip either slips or is pinned, depending on the force from the substrate, $\vec{\mathcal{F}} = (\mathcal{F}_x, \mathcal{F}_y)$, the coefficient of static friction, μ, and the vertical height y_0. (b) Photograph of the slip motion of a strip (for illustrative purposes only).

elastica problems [41–43]. First, we numerically investigate the planar deformations of a strip in the absence of gravity by changing the values of the coefficient of static friction, μ, and the height of the strip, y_0, and classify the deformations into three distinct states explained below. These morphologies, as well as the shape transitions between them, are confirmed by our experiments. An analytic model based on geometrically exact Kirchhoff rod equations combined with the static friction law is then developed, which accurately predicts the onset of slip events observed in the simulations. Finally, we explore the effect of gravity to discuss how our system may approach those studied in the context of elastic rope coiling [23,24].

Simulations.—To investigate the planar deformation of a strip with slip in a geometrically nonlinear regime, we performed systematic numerical simulations using a discrete analog of the continuum elastica model [44]. A full detail of our numerical method is given in Supplemental Material [45].

The top end of the strip is clamped along the vertical (y) axis. Generally, when the strip's tip is in contact with the substrate, the tip experiences forces and moments from the substrate but is otherwise free. In this study, we assume moment-free boundary conditions at the tip, even when in contact with the substrate. The force from the substrate is determined according to Eq. (1) [33]. Once $|\mathcal{F}_x|$ exceeds $\mu\mathcal{F}_y$, the kinetic friction force $\mu_k\mathcal{F}_y$ takes over, acting to oppose the continued slipping of the strip. As soon as the tangential force falls below this threshold, the static friction sets in again. We confirmed that our results are insensitive to a precise static-kinetic switching protocol (see our Supplemental Material for further details [45]).

We change the position of the clamped end at a given speed, so that the strip of initial length L is pushed against the substrate from directly above, until its height reaches a given value $y_0(< L)$. The stretching modulus is set to a sufficiently large value, in order to restrict the typical variation in arc length to within a few percent. Similarly, the velocity of the clamped end is chosen to be sufficiently small when compared to the bending relaxation time [45], in order to minimize any protocol-dependent kinetic effects. Throughout this work, we use a kinetic and static frictional coefficient ratio of $\mu_k/\mu = 0.8$, which is valid for typical surfaces.

Slip morphology of elastica.—We consider a planar bending deformation of a straight strip of length L, characterized by a radius of curvature, R. The bending torque is EI/R, where E is Young's modulus and I is the moment of inertia of the strip. Since the typical displacement perpendicular to the strip axis is L^2/R, the gravitational torque acting on the strip is $\rho g L^3/R$, where ρ represents the mass *per unit length* along the strip center line. Balancing the two torques provides a so-called "gravito-bending length" [24,41]:

$$L_g = \left(\frac{EI}{\rho g}\right)^{1/3}. \tag{2}$$

The dimensionless parameter L/L_g quantifies the relative importance of gravity to the elasticity. For $L/L_g \gg 1$, the strip is significantly deformed by gravity (i.e., by its own weight), and this scenario has been extensively studied previously [24,41]. Here, we are interested in the opposite limit $L/L_g \ll 1$, in which the behavior of a stiff strip is effectively studied by neglecting gravitational body forces. Our systematic numerical investigations in this regime are summarized in a phase diagram in Fig. 2. The shapes are classified as pinned (P) (for large μ and small $\epsilon_y \equiv 1 - y_0/L$), partially slipped (PS) (for large μ and large ϵ_y), and completely slipped (CS) (for small μ and large ϵ_y) states. If the tip remains stationary, it is said to be a P state; if it slips, and the final shape has an inflection point, it is a PS state; otherwise, it is a CS state. The phase diagram in Fig. 2 is constructed according to this protocol [45]. We find clear boundaries between the three regions in Fig. 2, which we now rationalize using the exact theory of elastica and scaling arguments.

Phase boundaries.—The diagram in Fig. 2 suggests that, between the P and CS states, the coefficient of static friction assumes a critical value, which depends on the vertical strain ϵ_y, i.e., $\mu_c = \mu_c(\epsilon_y)$. The geometry of our analytic theory is shown in Fig. 1(a), where the unit tangent is parameterized as $\vec{t}(s) = (\sin\theta(s), -\cos\theta(s))$, using the variable $\theta(s)$, where s is the arc length measured from the clamped top, $s = 0$. The relevant boundary conditions are thus written as $\theta(0) = 0$ and $\theta'(L) = 0$, where the prime symbol represents the derivative with respect to s. This latter boundary condition suggests that no external moment

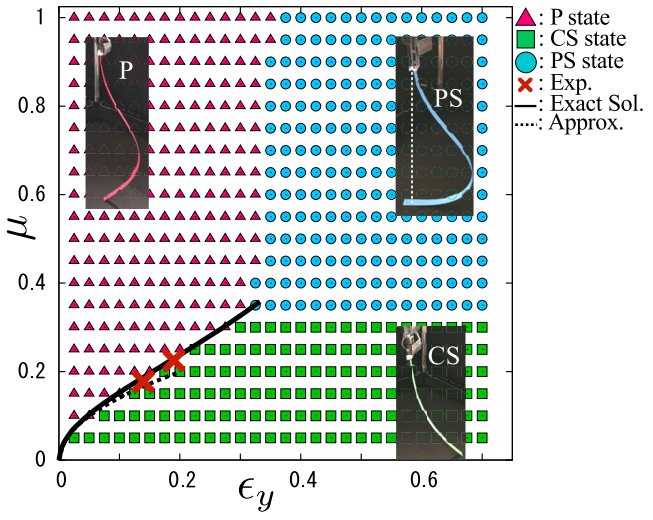

FIG. 2. Phase diagram of the equilibrium planar shapes of a strip in the (ϵ_y, μ) parameter space, constructed from numerical simulations for compressive protocols in the absence of gravity. Two different experimental data points are plotted as the thick red × symbols. The solid line represents the theoretical prediction based on the exact solution for the elastica curve, and the dashed line is its approximation given by Eq. (3). Note that the theoretical curve ends when the areal contact begins and the elastica solution no longer exists.

is applied at the end of the strip. We now let $\vec{F}(s)$ and $\vec{M}(s)$ be the internal force and moment, respectively, over the cross section of a strip at the position s, and which are exerted by the section of the strip with an arc length greater than s on the section of the strip with an arc length less than s [46,47]. In the absence of any external forces and moments, the force balance of an elastica is described by the Kirchhoff rod equations [38,39] $\vec{F}'(s) = 0$ and $\vec{M}'(s) + \vec{t}(s) \times \vec{F}(s) = 0$ and the linear constitutive relation $\vec{M}(s) = EI\theta'(s)\hat{e}_z$. Both tangential and vertical external forces must be applied at the clamped end, i.e., $\vec{F}(0) = (\mathcal{F}_x, \mathcal{F}_y)$, where $\mathcal{F}_x$ and $\mathcal{F}_y$ are yet to be determined. Solving the force-balance equation with this condition and substituting it into the momentum balance equation leads us to the shape equation for $\theta(s)$ [42,43], which may be written as $EI\theta''(s) = -\mathcal{F}_x \cos\theta(s) - \mathcal{F}_y \sin\theta(s)$. Although the equation for $\theta(s)$ can be analytically solved using elliptic integrals [48–50], the result for small strain, $\epsilon_y \ll 1$, is useful for our aim here [45]. Further details are found in Supplemental Material [45]. Combining it with the slip condition for $\vec{\mathcal{F}}$ in Eq. (1), we arrive at

$$\mu_c(\epsilon_y) = \frac{|\mathcal{F}_x|}{\mathcal{F}_y} \simeq 0.445\sqrt{\epsilon_y}. \tag{3}$$

This approximate solution matches the exact elliptic function solution [50] quite well for $\epsilon_y \ll 1$ and is in excellent agreement with the numerical data, as seen in Fig. 2. The shape reconstructed from the approximate solution is shown in Fig. 4(a) and describes the configurations observed in our simulations and experiments (outlined below) quite well.

The boundary between the P and PS states in the phase diagram (Fig. 2) suggests that a maximum vertical strain $\epsilon_y^{\max}$ exists for the P state, which is *independent* of μ, for large μ. This observation is corroborated on the basis of the following simple argument. Once $\theta(L)$ reaches $\pi/2$, a P configuration may be permanently stabilized, because the contact area between the strip and the surface increases with any further compressive force. Assuming then that the shape of the bent strip is close to that of a semicircle of radius R_{eff} [see Fig. 4(b)] and regarding $\pi R_{\text{eff}} \simeq L$, we obtain $\epsilon_y^{\max} \simeq (L - 2R_{\text{eff}})/L \simeq 1 - 2/\pi \simeq 0.363$. This rough argument yields a surprisingly good prediction for the position of the phase boundary between the P and PS states in Fig. 2.

Interestingly, our diagram in Fig. 2 suggests the existence of the triple point at $(\epsilon_{y,\text{tp}}, \mu_{\text{tp}}) \simeq (0.325, 0.35)$. Because the P-CS and P-PS boundary lines meet at this particular point, it is uniquely determined by finding the condition of the P-CS transition in the limit of $\theta(L) = \pi/2$, i.e., at the onset of areal contact. This predicts that $\mu_{\text{tp}} \simeq 0.35$ is a universal, geometry-ruled constant, independent of elastic constants. Therefore, for substrates with $\mu > \mu_{\text{tp}}$, the slip instability, which can induce an abrupt, often unpredictable motion of a strip, should always be suppressed. Such a practical guideline could be useful in industrial designs of safe and stable operations of slender structures in contact with surfaces.

Experiments.—To verify our main theoretical findings, we conducted controlled physical experiments using a slender elastic strip made of polyvinyl chloride (PVC) of length $L = 150$ mm, width 10 mm, and thickness 1 mm. The Young's modulus of such a PVC strip is known to be $E = 2.4$–4.1×10^9 Pa, and the gravito-bending length L_g in our experiments is estimated as 240–310 mm, which exceeds the total length of the strip L. The bottom and side faces of our strip were polished with sandpaper to add some surface roughness, and two types of substrates—an aluminum plate and a carbon black-filled natural rubber sheet—were used to vary the frictional coefficients in a controlled manner. In the experiments, the head of the z-stage clamping the PVC strip moved downward sufficiently slowly by a distance of 1%–2% of the strip's length. At every step, the clamping end was kept fixed for 30 s so that the strip attained its equilibrium position, after which the *total* tangential and horizontal forces that the strip exerted on the substrate were measured. See our Supplemental Material for full experimental details [45].

In Figs. 3(a) and 3(b), the experimental force vs strain relations are plotted, together with those predicted from our simulations. The forces are rescaled in units of EI/L^2. We find an excellent agreement between the simulation and experiment, from which we could estimate $\mu \simeq 0.225$, for the case in Fig. 3(a) [51]. This particular experimental point, $(\epsilon_y, \mu) = (0.19, 0.225)$, as well as data from another experiment, $(\epsilon_y, \mu) = (0.14, 0.175)$, are superposed on the diagram in Fig. 2. The two data points sit exactly on the

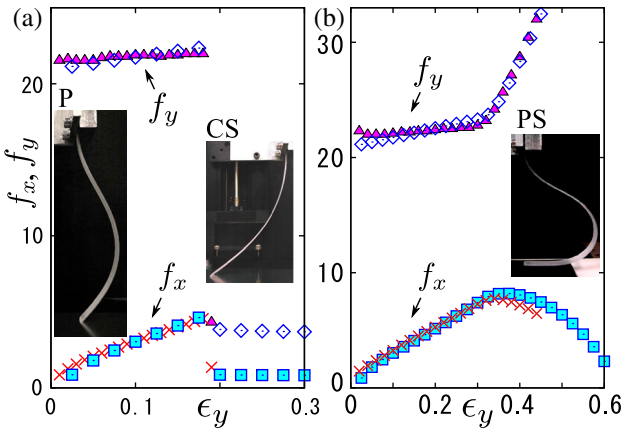

FIG. 3. Rescaled total tangential (f_x) and normal (f_y) forces acting on a strip by the substrate, measured in simulations and experiments and plotted as a function of the vertical strain ϵ_y. (a) f_x (×) and f_y (triangle) from the experiment with an aluminum surface. f_x (square) and f_y (diamond) from simulations with $\mu = 0.225$. (b) f_x (×) and f_y (triangle) from the experiment with a rubber surface. f_x (square) and f_y (diamond) from simulations with $\mu = 0.40$. Insets in (a) and (b) are the experimental snapshots for P ($\epsilon_y = 0.10$), CS ($\epsilon_y = 0.19$), and PS ($\epsilon_y = 0.40$).

phase boundary between P and CS predicted from simulations and our theoretical analysis.

In the experiment with the aluminum plate [Fig. 3(a)], we observed the transition to the CS state. In this case, the tangential and normal forces increase as the strip buckles, and at the slip transition, these forces experience an abrupt and discontinuous decrease in strength. In contrast, the PS state occurs in the experiments with the rubber substrate [Fig. 3(b)], where the force curves are distinct from those in the CS case. Across the transition to the PS state, the normal force starts to increase in magnitude, while the tangential force begins to decrease continuously. A closer look at this event reveals that the partial slip involves the onset of the areal contact between the strip and the substrate. This geometric transition is continuous and acts to reduce the tangential tension while increasing the normal force significantly.

Surprisingly, the force response in our simulation is found *independent* of μ in the P-PS regime [51]; in Fig. 3(b), we show the numerical data for $\mu = 0.4$, but the data with other $\mu(> \mu_{\rm tp})$ fit equally well to the experiment. This property precludes a comparison between the simulation and experiment and, thus, an estimation of the experimental value of μ. By the nature of contact friction, it is technically difficult to know values of μ ahead of measurements. Thus, an experimental verification of the predicted triple point is inaccessible, as it requires the systematic control of μ as an input parameter. A more elaborate technique could overcome this difficulty [52–54], which, however, is beyond the scope of the present study.

Hysteresis.—In Fig. 4(c), the position of the free end, or the slip distance, $x(s = L) = x_{\rm end}$, obtained from our simulations is plotted as a function of ϵ_y for $\mu = 0.2$ [45]. A discontinuous change in $x_{\rm end}/L$ at the transition from the P to the CS state appears in Fig. 4(c), whereas $x_{\rm end}$ changes continuously from zero at the transition from the P to the PS state (data not shown). Furthermore, Fig. 4(d) shows that the trajectory of $x_{\rm end}$ in the reverse process differs considerably from that of the compression process, revealing a distinct hysteresis in the cyclic process. In particular, the strip never returns to the P configuration in the reversed process [45]. We show the phase diagrams generated by the reverse processes in Fig. 4(e), where no P state exists. Such protocol-dependent hysteretic behavior, or multistability, is a direct consequence of the friction law and has also been found in granular experiments under shear [55].

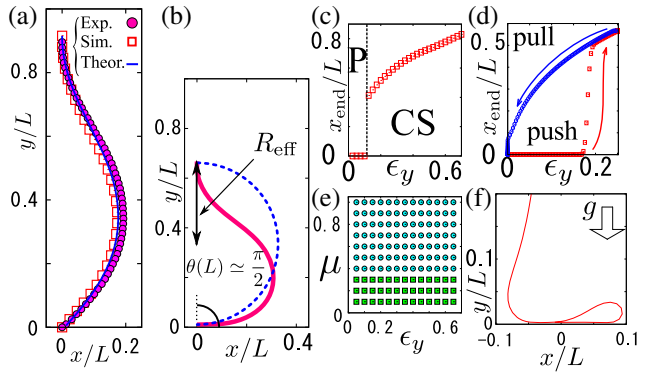

FIG. 4. (a) Comparison of the simulation (square) for $\mu = 1.0$, the experiment (circle), and the analytic theory (solid line) for P states with $\epsilon_y = 0.10$. (b) Critical P configuration (from the simulation) close to the P-PS boundary, $(\epsilon_y, \mu) = (0.35, 1.0)$. (c) Rescaled slip distance $x_{\rm end}/L$, plotted as a function of ϵ_y, obtained from the simulations for $\mu = 0.2$ during the compression process. (d) $x_{\rm end}/L$, plotted as a function of ϵ_y, with $\mu = 0.2$ for compression (squares) and reverse (circles) processes. The working speed here is twice as fast as that in (c). (e) Phase diagram for the reverse protocols. The symbols are the same as ones in Fig. 2. (f) Self-folding for $L/L_g \simeq 6$ obtained from simulations for $(\epsilon_y, \mu) = (0.15, 0.2)$.

Effect of gravity.—We now discuss the effect of gravity by changing the dimensionless ratio L/L_g while fixing $(\epsilon_y, \mu) = (0.15, 0.2)$, so that the strip is in the P configuration for $g = 0$. As L/L_g is increased, the strip tends to sag, while for $L/L_g = O(1)$, i.e., when the bending is comparable to the gravity, the free end slips easily, because the effect of gravity acts to increase $\theta(L)$, and the horizontal force $\mathcal{F}_x$ also increases. However, the resulting shape is distinct from that of the CS state, because the strip interacts with the substrate by areal contact rather than point contact. As L/L_g becomes larger [$L/L_g \simeq 6$ in Fig. 4(f)], the strip folds and loops back on itself. This folding is analogous to the planar version of an elastic rope coiling. Actually, using the same parameter set, we can reproduce a realistic coiling shape in our three-dimensional simulation of a twist-free elastic string [45]. We here suggest the following physical scenario about the initiation of the coiling. First, the free end slips partially immediately upon contact with the substrate. Subsequently, the contact length increases monotonically as the string sags, which significantly reduces the tangential tension and prevents the string from slipping further. This effectively confines the sagging string to a localized position, eventually leading to the characteristic coiling.

Conclusion.—We investigated the planar slip configurations of an elastic strip pushed onto a frictional rigid substrate. Combining numerical, analytical, and experimental approaches, we revealed the fundamental aspects of this problem in the limit of weak gravitational effects and quantified the relative importance of the system's geometry, elasticity, friction, and gravity. The framework presented here could be applied to a number of biophysical phenomena across different scales, including membrane-bound actin polymerization in cell motility [56,57], gravity-guided intrusion of plant roots in soil [8,9], and contact mechanics of the adhesive hairs in geckos' toe pads [27–31]. In all of these examples, bending of thin elastic objects against rigid or flexible substrates occurs, determining the overall behavior. This suggests a profound connection between the mechanical processes and the specific biological functions in those systems. Our formalism needs to be modified to account for other physical aspects such as spontaneous curvature, surface chemistry, or active changes of them. However, the mechanism of the friction-controlled buckling and slippage is generic and will provide a robust

physical basis for understanding a range of complex biophysical problems.

We acknowledge financial support from Grants-in-Aid for Japan Society for the Promotion of Science (JSPS) Fellows (Grant No. 28·5315) and JSPS KAKENHI (No. 15H03712 and No. 16H00815: "Synergy of Fluctuation and Structure: Quest for Universal Laws in Non-Equilibrium Systems," and No. JP16H06478: "Science of Slow Earthquakes").

[1] D'Arcy W. Thompson, *On Growth and Form: The Complete Revised Edition* (Dover, New York, 1992).
[2] S. Ghosal, Phys. Rev. Lett. **109**, 248105 (2012).
[3] L. Wolpert *et al.*, *Principles of Development* (Oxford University, New York, 1998).
[4] S. Höhn, A. R. Honerkamp-Smith, P. A. Haas, P. K. Trong, and R. E. Goldstein, Phys. Rev. Lett. **114**, 178101 (2015).
[5] J. Sachs, *Text-book of Botany, Morphological and Physiological* (Clarendon, Oxford, 1875).
[6] A. Goriely and M. Tabor, Phys. Rev. Lett. **80**, 1564 (1998).
[7] J. Engelberth, Adv. Space Res. **32**, 1611 (2003).
[8] G. D. Massa and S. Gilroy, Plant J. **33**, 435 (2003).
[9] G. B. Moushausen, T. N. Bibikova, M. H. Weisenseel, and S. Gilroy, Plant Cell **21**, 2341 (2009).
[10] P. Pieranski, S. Kasas, G. Dietler, J. Dubochet, and A. Stasiak, New J. Phys. **3**, 10 (2001).
[11] A. M. Menzel and N. Goldenfeld, Phys. Rev. E **84**, 011122 (2011).
[12] J. Dumais and Y. Forterre, Annu. Rev. Fluid Mech. **44**, 453 (2012).
[13] K. Jin, J. Shen, R. W. Ashton, I. C. Dodd, M. A. J. Parry, and W. R. Whalley, J. Exp. Bot. **64**, 4761 (2013).
[14] J. P. Steimel, J. L. Aragones, and A. Alexander-Katz, Phys. Rev. Lett. **113**, 178101 (2014).
[15] A. Ward, F. Hilitski, W. Schwenger, D. Welch, A. W. C. Lau, V. Vitelli, L. Mahadevan, and Z. Dogic, Nat. Mater. **14**, 583 (2015).
[16] R. E. Goldstein, P. B. Warren, and R. C. Ball, Phys. Rev. Lett. **108**, 078101 (2012).
[17] A. C. Callan-Jones, P.-T. Brun, and B. Audoly, Phys. Rev. Lett. **108**, 174302 (2012).
[18] M. K. Jawed, P. Dieleman, B. Audoly, and P. M. Reis, Phys. Rev. Lett. **115**, 118302 (2015).
[19] D. Vella, A. Boudaoud, and M. Adda-Bedia, Phys. Rev. Lett. **103**, 174301 (2009).
[20] J. M. Kolinski, P. Aussillous, and L. Mahadevan, Phys. Rev. Lett. **103**, 174302 (2009).
[21] L. Mahadevan and J. B. Keller, Proc. R. Soc. A **452**, 1679 (1996).
[22] N. M. Ribe, Phys. Rev. E **68**, 036305 (2003).
[23] M. Habibi, N. M. Ribe, and D. Bonn, Phys. Rev. Lett. **99**, 154302 (2007).
[24] M. K. Jawed, F. Da, J. Joo, E. Grinspun, and P. M. Reis, Proc. Natl. Acad. Sci. U.S.A. **111**, 14663 (2014).
[25] P.-T. Brun, B. Audoly, N. M. Ribe, T. S. Eaves, and J. R. Lister, Phys. Rev. Lett. **114**, 174501 (2015).
[26] J. Klein, E. Kumacheva, D. Mahalu, D. Perahia, and L. J. Fetters, Nature (London) **370**, 634 (1994).
[27] R. J. Full, K. Autumn, Y. A. Liang, S. Tonia Hsieh, W. Zesch, W. P. Chan, T. W. Kenny, and R. Fearing, Nature (London) **405**, 681 (2000).
[28] L. Ge, S. Sethi, L. Ci, P. M. Ajayan, and A. Dhinojwala, Proc. Natl. Acad. Sci. U.S.A. **104**, 10792 (2007).
[29] N. Gravish, M. Wilkinson, and K. Autumn, J. R. Soc. Interface **5**, 339 (2008).
[30] B. Chen, P. D. Wu, and H. Gao, Proc. R. Soc. A **464**, 1639 (2008).
[31] N. Gravish *et al.*, J. R. Soc. Interface **7**, 259 (2010).
[32] J. T. Miller, T. Su, E. B. Dussan V., J. Pabon, N. Wicks, K. Bertoldi, and P. M. Reis, Int. J. Solids Struct. **72**, 153 (2015).
[33] B. N. J. Persson, *Sliding Friction* (Springer-Verlag, Berlin, 2000).
[34] N. Stoop, F. K. Wittel, and H. J. Herrmann, Phys. Rev. Lett. **101**, 094101 (2008).
[35] S. M. Rubinstein, G. Cohen, and J. Fineberg, Nature (London) **430**, 1005 (2004).
[36] M. Otsuki and H. Matsukawa, Sci. Rep. **3**, 1586 (2013).
[37] H. Alarcón, T. Salez, C. Poulard, J.-F. Bloch, É. Raphaël, K. Dalnoki-Veress, and F. Restagno, Phys. Rev. Lett. **116**, 015502 (2016).
[38] L. D. Landau and E. M. Lifshitz, *Theory of Elasticity* (Pergamon, Oxford, 1980).
[39] B. Audoly and Y. Pomeau, *Elasticity and Geometry* (Oxford University, New York, 2010).
[40] L. Euler, Mem. Acad., Berlin **13** (1759).
[41] C. Y. Wang, Int. J. Mech. Sci. **28**, 549 (1986).
[42] X. Q. He, C. M. Wang, and K. Y. Lam, Archive of Applied Mechanics **67**, 543 (1997).
[43] R. H. Plaut, D. A. Dillard, and A. D. Borum, J. Appl. Mech. **78**, 041011 (2011).
[44] G. Chirico and J. Langowski, Biopolymers **34**, 415 (1994).
[45] See Supplemental Material at http://link.aps.org/supplemental/10.1103/PhysRevLett.118.178001 for for details of simulations, full experimental details, and analytic calculations.
[46] M. Nizette and A. Goriely, J. Math. Phys. (N.Y.) **40**, 2830 (1999).
[47] T. R. Powers, Rev. Mod. Phys. **82**, 1607 (2010).
[48] Y. Mitaka, Acta Mech. **190**, 133 (2007).
[49] M. Abramowitz and I. A. Stegun, *Handbook of Mathematical Functions: With Formulas, Graphs, and Mathematical Tables* (Dover, New York, 1964).
[50] T. G. Sano and H. Wada (to be published).
[51] A creeplike slip due to the areal contact underlies this μ independence, but its detailed analysis is beyond the scope here and will be published in Ref. [50].
[52] T. Tominaga, N. Takedomi, H. Biederman, H. Furukawa, Y. Osada, and J. P. Gong, Soft Matter **4**, 1033 (2008).
[53] M. Takata, T. Yamaguchi, J. P. Gong, and M. Doi, J. Phys. Soc. Jpn. **78**, 084602 (2009).
[54] R. Suzuki, T. Yamaguchi, and M. Doi, J. Phys. Soc. Jpn. **82**, 124803 (2013).
[55] S. Nasuno, A. Kudrolli, and J. P. Gollub, Phys. Rev. Lett. **79**, 949 (1997).
[56] A. Mogilner and G. Oster, Biophys. J. **71**, 3030 (1996).
[57] D. R. Daniels, D. Marenduzzo, and M. S. Turner, Phys. Rev. Lett. **97**, 098101 (2006).